Stellar populations in bulges The isolated galaxies

L. Morelli[1], L. Costantin[2], E.M. Corsini[2], E. Dalla Bontà[2], L. Coccato[3], J. Méndez-Abreu[4] & A. Pizzella[2]

[1] *Instituto de Astronomía y Ciencias Planetarias Universidad de Atacama, Copiapó, Chile*
[2] *Dipartimento di Fisica e Astronomia "G. Galilei", Università di Padova, Italy*
[3] *European Southern Observatory, Garching, Germany*
[4] *Instituto Astrofísico de Canarias, La Laguna, Spain*

Contact / lorenzo.morelli@uda.cl

Resumen / En una reciente serie de artículos se han presentado los resultados de la investigación sobre la población estelar y sus gradientes en las regiones de la galaxias donde la luz esta dominada por el bulbo.
En la presentación oral se han mostrado los resultados de estos trabajos y los últimos avances del proyecto, mostrando las propriedades de la población estelar en el bulbo de galaxias en ambiente aislado.

Abstract / In a recent series of papers we presented the results of the investigation on the stellar populations and their gradients of the bulge dominated region.
The results of these works have been presented in the talk along with the last progresses in this projects, showing the properties of the stellar populations in the bulge dominated regions of galaxies in isolated environment.

Keywords / galaxies: abundances — galaxies: bulges — galaxies: formation — galaxies: kinematics and dynamics — galaxies: spiral — galaxies: stellar content

1. Introducción

Most of the stars in the local universe reside in the bulges of disk galaxies. Their morphological classification is based on the relative prominence of the spheroidal and disk components and their structures reflects the different formation processes. Thus, it follows that understanding how bulges assembled is a crucial step in understanding galaxy formation.

Dissipative collapse (e.g., Gilmore & Wyse, 1998), major and minor merging events (e.g., Cole et al., 2000), and redistribution of disk material due to the presence of a bar or environmental effects (e.g., Kormendy & Kennicutt, 2004) drives to the variety of properties observed in bulges. Theoretical models give strong constraints on the resulting galaxy that need to be tested with observations. In particular, an invaluable piece of information to understand the processes of formation and evolution of galaxies is imprinted in their stellar populations (e.g., Seidel et al., 2015; McDermid et al., 2015; Corsini et al., 2018) and even more in their radial gradients (e.g., Gorgas et al., 2007; Morelli et al., 2008; González Delgado et al., 2014; Morelli et al., 2015b) since different formation scenarios predict different radial trends of age, metallicity, and alpha/Fe enhancement.

To take on this challenge we have started a campaign to investigate the stellar populations of bulges of galaxies residing in dense environments to compare their nature with the nature of bulges in isolated galaxies.

In Morelli et al. (2008, 2012, 2015a) the central value and radial gradient of age, metallicity, and [α/Fe] enhancement has been measured for a large number of high-surface brightness (HSB) and low-surface brightness (LSB) galaxies. The only common feature for these bulges (independently from their morphological type and environment) is the negative metallicity gradient along the galaxy radius. All these characteristics are supporting scenarios like violent relaxation due to a merging event, or dissipative collapse in monolithic scenario and discourage secular evolution. However, secular evolution could still be the main responsible for the formation of galaxies with small bulges (Costantin et al., 2017, 2018). The variety of the results testifies the complexity of the topic and could be due to the continuous interactions between the cluster galaxies and their dense environment (Corsini et al., 2017).

2. Isolated bulges

A way to make the observational picture simpler is studying the bulges of isolated galaxies, for which the interactions with the surrounding environment or with other galaxies are likely to be negligible (Hirschmann et al., 2013).

In Morelli et al. (2016) we analysed the stellar populations of the bulges of a carefully selected sample of HSB isolated disk galaxies to be compared with the complementary samples of bulges in HSB cluster galaxies and giant LSB galaxies. In Fig. 1 we reported the comparison of morphological type, central velocity disper-

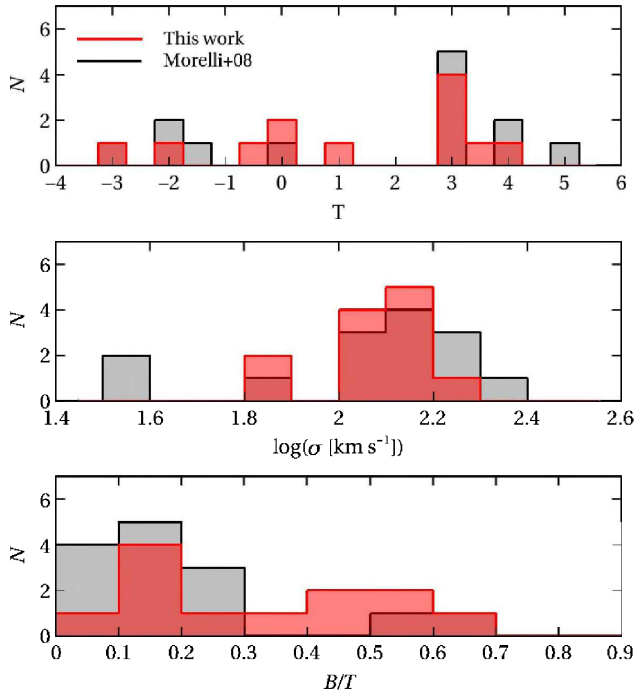

Figure 1: Distribution of the morphological type (upper panel), central velocity dispersion (middle panel), and B/D ratio (lower panel) for the sample galaxies (red histograms). The distribution of the same quantities for the group and cluster galaxies studied by Morelli et al. (2008) is plotted for a comparison (grey histograms).

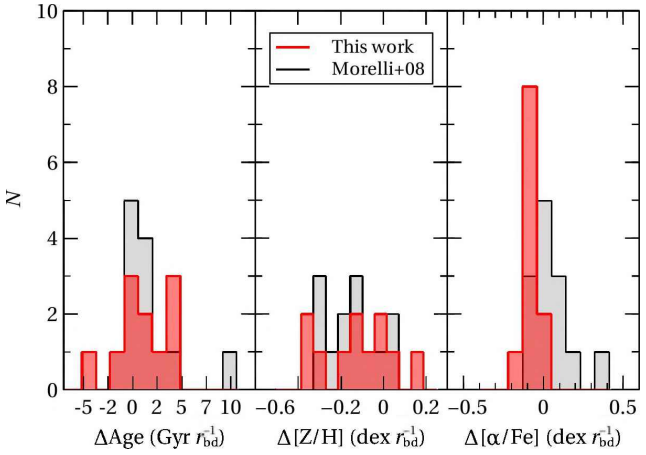

Figure 2: Distribution of the gradients of mean age (left-hand panel), total metallicity (central panel), and total α/Fe enhancement (right-hand panel) for the sample bulges (red histograms). The distribution of the same quantities for the bulges of group and cluster galaxies studied by Morelli et al. (2008) is plotted for a comparison (grey histograms).

sion, and B/D ratio between the two sample.

In order to measure the stellar populations gradients in the bulge we had to derive the relative importance of disc, bulge and bar along the radius. Their structural parameters were derived from the sky and mask-subtracted i-band images by applying the Galaxy Surface Photometry Two-Dimensional Decomposition (GASP2D) algorithm (Méndez-Abreu et al., 2008, 2014). Following the photometric decomposition we defined $r_{\rm bd}$, the radius where the surface brightness contribution of the bulge component is equal to the contribution from the other components.

The gradients of age, metallicity and α-enhancement were derived as the difference between the value derived at radius $r_{\rm bd}$, and the central value obtained within $0.1r_{\rm e}$. We confirm the negative radial trend in metallicity also for the isolated galaxy, but the main result is the negative gradient for the [α/Fe] enhancement (Fig. 2).

3. Conclusions

We analysed the surface-brightness distribution, stellar kinematics, and stellar population properties of a sample of isolated galaxies selected from the Catalogue of Isolated Galaxies (Karachentseva, 1973), to constrain the dominant mechanism of the assembly of their bulges. We give particular attention to the stellar populations gradient along the radius of the galaxy.

All the sample bulges show a negative gradient for the α/Fe enhancement. This is a prediction of the dissipative collapse model for bulge formation and it has never been observed before. We suggest that the gradients imprinted during the inside-out formation process are preserved in the bulges of isolated galaxies, which suffered a limited number of interactions and mergers, whereas the gradients are cancelled in the bulges of group and cluster galaxies as a consequence of phenomena driven by environment.

Acknowledgements: This investigation was based on observations obtained at the ESO Telescopes at the La Silla Paranal Observatory under programmes 76.B-0375, and 80.B-00754. This work was partially supported by Padua University through grants 60A02-5857/13, 60A02-5833/14, 60A02-4434/15, and CPDA133894. LM acknowledges financial support from Padua University grant CPS0204. JMA acknowledges support from the European Research Council Starting Grant SEDmorph (P.I. V. Wild).

References

Cole S., et al., 2000, MNRAS, 319, 168
Corsini E.M., et al., 2017, MNRAS, 466, 974
Corsini E.M., et al., 2018, A&A, 618, A172
Costantin L., et al., 2017, A&A, 601, A84
Costantin L., et al., 2018, MNRAS, 481, 3623
Gilmore G., Wyse R.F.G., 1998, AJ, 116, 748
González Delgado R.M., et al., 2014, A&A, 562, A47
Gorgas J., Jablonka P., Goudfrooij P., 2007, A&A, 474, 1081
Hirschmann M., et al., 2013, MNRAS, 433, 1479
Karachentseva V.E., 1973, Soobshch. Spets. Astrofiz. Obs., 8, 3
Kormendy J., Kennicutt R.C., 2004, ARA&A, 42, 603
McDermid R.M., et al., 2015, MNRAS, 448, 3484
Méndez-Abreu J., et al., 2008, A&A, 478, 353
Méndez-Abreu J., et al., 2014, A&A, 572, A25
Morelli L., et al., 2008, MNRAS, 389, 341
Morelli L., et al., 2012, MNRAS, 423, 962
Morelli L., et al., 2015a, Astron. Nachr., 336, 208
Morelli L., et al., 2015b, MNRAS, 452, 1128
Morelli L., et al., 2016, MNRAS, 463, 4396
Seidel M.K., et al., 2015, MNRAS, 451, 936

Origin of high ionization lines in active galactic nuclei

Y. Diaz[1,2] & A. Rodríguez-Ardila[3,4]

[1] *Instituto Nacional de Pesquisas Espaciais/MCTI, São Jose dos Campos, SP, Brazil*
[2] *Instituto de Física y Astronomía, Facultad de Ciencias, Universidad de Valparaíso, Valparaíso, Chile*
[3] *Laboratorio Nacional de Astrofísica/MCTI, Itajubá, MG, Brazil*
[4] *Instituto de Astrofísica de Canarias, La Laguna, Tenerife, Spain*

Contact / yaherlyn.diaz@postgrado.uv.cl

Resumen / Presentamos evidencias de que la fotoionización por radiación de la fuente central no puede explicar la emisión de líneas coronales observadas en los núcleos galácticos activos (AGN, por sus siglas en inglés). Encontramos que la emisión coronal en los objetos estudiados se extiende a distancias de hasta 150–200 pc y es coespacial con el *jet* de radio. Los modelos de fotoionización de CLOUDY muestran que la fotoionización no es el único mecanismo físico responsable de la emisión de líneas coronales. Otros procesos como los choques son necesarios para explicar la emisión del gas de alta ionización. En general, nuestro trabajo destaca la necesidad de observaciones IFU con alta resolución angular, para comprender, con mayor precisión, los procesos físicos que ocurren en los parsecs centrales de las AGNs.

Abstract / We present strong evidence that the photoionization by radiation from the central engine cannot explain the emission of Coronal lines observed in Active Galactic Nuclei (AGN). We found that the coronal emission in the studied objects is extended to distances of up to 150–200 pc and co-spatial with the radio jet. Photoionization models of CLOUDY show that photoionization is not the only physical mechanism responsible for the emission of coronal lines. Another processes such as shocks are necessary to explain the emission of the high ionization gas. Overall, our work highlights the need of high angular IFU observations to understand, more accurately, the physical processes associated to the central few parsecs in AGNs.

Keywords / galaxies: nuclei — galaxies: kinematics and dynamics — techniques: spectroscopic

1. Introduction

Active galactic nuclei (AGNs) present, in their spectra, lines of high ionization or coronal lines (CLs). Due to the potential necessary for its production (>100 eV), the CLs trace a part of the ionizing continuum which is not always directly accessible from observations due to galactic absorption. It is known that CLs are generally emitted in compact regions near the central source, but the physical conditions of the gas and the mechanisms associated with its production are under discussion.

In this work we analyze the most internal parsecs of a sample of four nearby active galaxies with prominent coronal emission to study the physical mechanisms responsible for the production of CLs. For this purpose, observations of high angular resolution ($\sim$ 0.1" px^{-1}) collected with integral field spectroscopy and adaptive optics (AO) allowed the study of the spatial distribution of the high ionization gas and model the reasons [Si VI]/Brγ, [S IX]/Paβ, [Ca VIII]/Brγ and [S VIII]/Paβ using CLOUDY. The width, shape of the profiles, and position of the centroid lines are additional diagnostics used to determine the contribution of energy processes such as outflows and shocks between the jets and the Narrow Line Region (NLR) gas.

2. Observations

- Four nearby active galaxies with prominent coronal emission: NGC 1068, NGC 1386, NGC 4151 and ESO 428-G014
- Observations with AO using NIFS/Gemini and SINFONI/VLT
- High-quality spectroscopic data spatially resolved at smaller scales of 0.15" px^{-1}, that translate to a angular scale of $\sim$ 15"px^{-1}.

For this work, we use galaxies with multiwavelength data, because this allows a more complete analysis of the physics associated to the gas. In addition, we select objects with evidence of the presence of outflows and extended coronal emission.

3. Morphology and extension of the Coronal line Region

Visual inspection of Fig. 1 shows that the region emitting [Si VI]λ1.963μm and Brγ for ESO 428-G14 is highly inhomogeneous and elongated along the NE-SW direction. The gas morphology is extended, reaching up to 195 pc to the SE and 110 pc to the NW. It forms a bright spot at NW that can be associated with an helical–shape. These are best seen in the Brγ image. This gas distribution is also reported by May et al. (2018).

Fig. 2 shows the flux map of the AGN NGC 1386. The morphology of the high ionization emitting gas

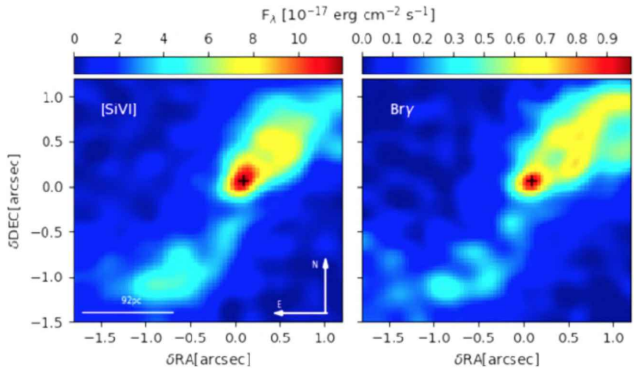

Figure 1: Flux distribution maps of [Si VI]λ1.962μm and Brγ for ESO 428-G14. The color bar indicates the values of integrated flux in units of 10^{-17} erg cm^{-2} s^{-1}. The orientation and spatial scale are the same for all panels.

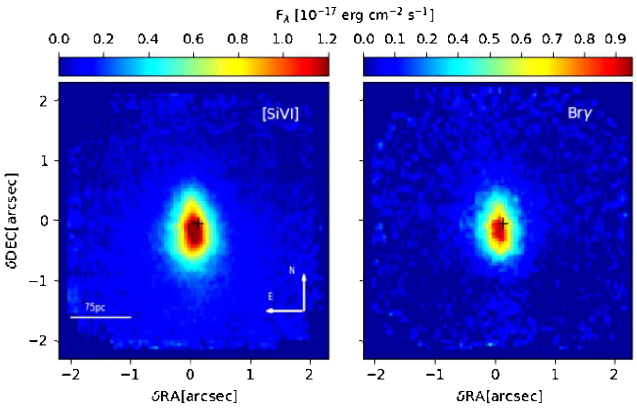

Figure 2: The same as Fig. 1 for NGC 1386.

[Si VI]λ1.963μm displays one prominent region of emission. It is characterized by a blob of $\sim$1" in radius, centered at the AGN and slightly elongated in the NS direction. The brightest region of this component is highly elongated in the NS direction, with a size of $\sim$1.2"$\times$0.6". This morphology was already observed by Rodríguez-Ardila et al. (2017). The morphology of Brγ emission is similar to the distribution observed for the high ionization line but with a shorter extension in the NS direction (0.5"$\times$0.5").

In Fig. 3, we overlapped the 2 cm radio map from VLA (Falcke et al., 1998) to the [Si VI] emissions and we found that the coronal gas is distributed along a PA very close to that of the radio jet, forming multiple filaments and knots of emission. This feature suggests a strong association between [Si VI] and the radio-jet: the jet plays a fundamental role in the morphology of the Coronal Line region (CLR) gas in ESO 428-G14. We defined the AGN location as the position where the K-band continuum emission (2.2 μm) peaks, which coincides with the maximum intensity of the [Si VI] emission. Also, X-ray observations obtained with *Chandra* show a PA similar to that of [Si VI] for this galaxy (May et al., 2018).

The CLs of ESO 4028-G14 display very intricate profiles, with multiple components and strong variations in their form and width from region to region. As an example, Fig. 4 shows the [Si VI] line profiles of spectra extracted from different spatial regions $\sim$0.2"$\times$0.2".

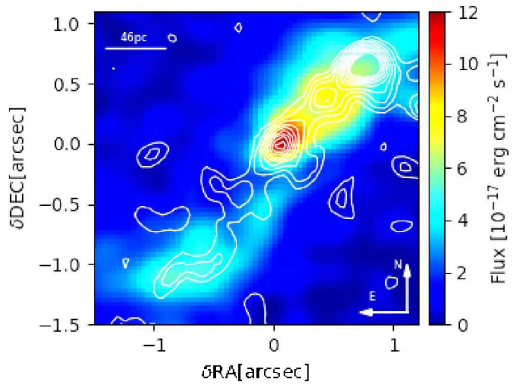

Figure 3: Flux distribution map of [Si VI]λ1.963μm overlaid with the VLA 2 cm radio emission for ESO 428-G14.

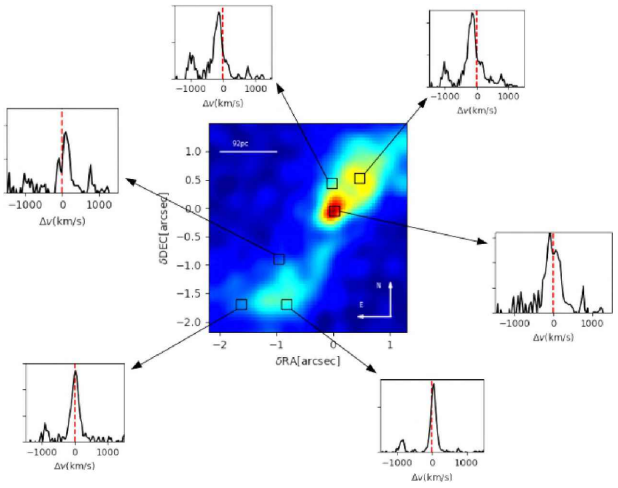

Figure 4: [Si VI] emission-line profiles for ESO 428-G14. The spectra were extracted from different spatial regions of $\sim$0.25$\times$0.25 arcsec^2. [Si VI] emission displays a very intricate profile, with multiple components and strong variations in their form and width from region to region.

4. Kinematics of the CLs

As can be seen in Fig. 5 and Fig. 6, [Si VI] is significantly broader than Brγ. Moreover, high-velocity clouds are observed at distances of up to $\sim$100 pc from the center and coincident with regions of strong radio emission, suggesting outflowing gas, probably due to interaction of the radio-jet with the interstellar medium.

5. Photoionization models

We investigate if photoionization by the central source alone is able to sustain highly ionized clouds at the distances detected in ESO 428-G14. To this aim, we run grids of photoionization models with CLOUDY Ferland et al. (version C17.01; 2017). The input parameters are

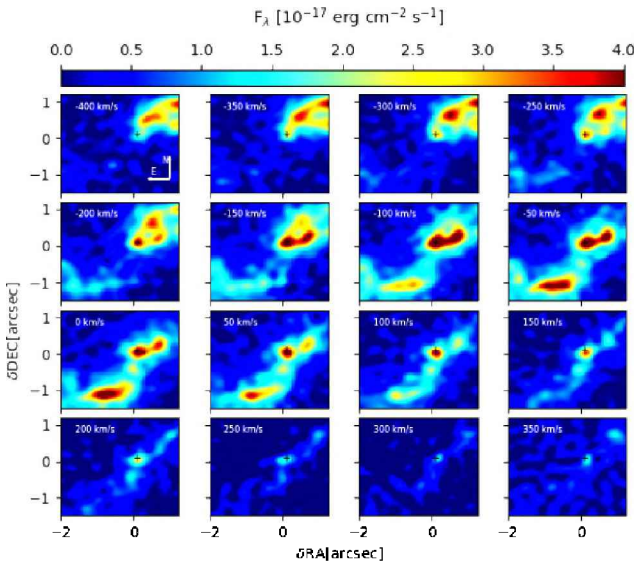

Figure 5: Channel maps derived for Brγ for ESO428-G14. A velocity bin of 50km s^{-1} is used to slice the data-cube. The color bar indicates the values of integrated flux in units of 10^{-17} erg cm^{-2} s^{-1}.

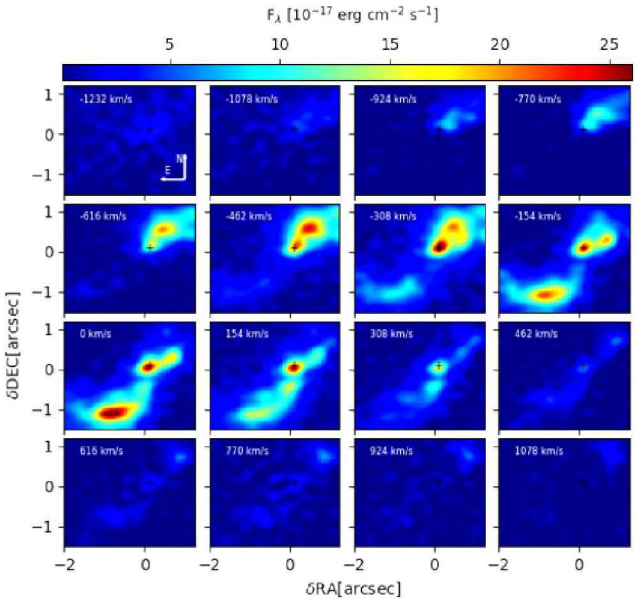

Figure 6: Channel maps derived for [Si VI] 1.963 μm for ESO428-G14. A velocity bin of 154kms^{-1} is used to slice the data-cube. The color bar indicates the values of integrated flux in units of 10^{-17} erg cm^{-2} s^{-1}.

the gas density, the distance of the clouds to the nucleus, the spectral energy distribution of the ionizing radiation ("Table AGN" command, similar to that deduced by Mathews & Ferland (1987), solar abundances and clouds with no dust. We used the total AGN luminosity (2×10^{42} erg s^{-1}).

The observed line ratios and the photoionization models are presented in Fig. 7. The extended gas distribution cannot be reproduced by photoionization by

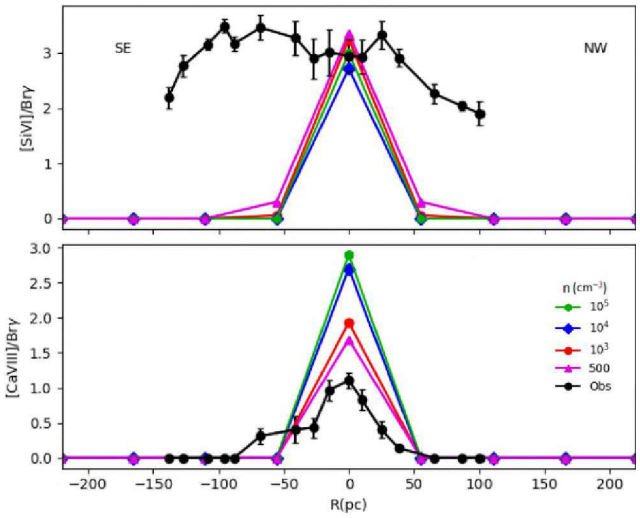

Figure 7: Predicted emission lines ratios [Si VI]/Brγ (upper panel) and [Ca VIII]/Brγ (bottom panel) for clouds with different densities (10^3 cm^3 red, 10^4 cm^3 blue, 10^3 cm^5 green and 500 cm^3 purple) for ESO 428-G14. The full circles are the observed line ratios.

the central source. Also, in May et al. (2018) we tested the scenario where the AGN luminosity is higher to explore the possibility of any potential AGN variability, and the result is the same. Also this previous scenario is observed for the whole sample. A combination of photoionization by the central source and shock excitation is necessary to explain the extended emission.

6. Conclusions

- For [Si VI] and Brγ in NGC 1386 the light distribution is compact and clearly resolved.
- For ESO 428-G14, [Si VI] is emitted by gas with a wide range of velocities, both positives and negatives, reaching values as high as $\sim$1000 km s^{-1} and ~ -1000 km s^{-1}. The gas in the central regions ($\sim$0.5 arcsec) is more turbulent, emitting at practically at all the displayed velocity range.
- Photoionization by radiation from the central engine is not able to explain the extended emission of high ionization gas. Another physical mechanism (such shocks) must be also considered to explain its large extended high–ionization region.

Acknowledgements: Diaz Y. thanks to CAPES and CONICYT PIA ACT172033 and A. Rodríguez-Ardila to CNPq.

References

Falcke H., Wilson A.S., Simpson C., 1998, ApJ, 502, 199
Ferland G.J., et al., 2017, RMxAA, 53, 385
Mathews W.G., Ferland G.J., 1987, ApJ, 323, 456
May D., et al., 2018, MNRAS, 481, L105
Rodríguez-Ardila A., et al., 2017, MNRAS, 470, 2845